

# Synthesis, characterization and biological activity of complexes of 2-hydroxy-3,5-dimethylacetophenoneoxime (HDMAOX) with copper(II), cobalt(II), nickel(II) and palladium(II)

Bibhesh K. Singh<sup>a</sup>, Umesh K. Jetley<sup>b</sup>, Rakesh K. Sharma<sup>a</sup>, Bhagwan S. Garg<sup>a,\*</sup>

<sup>a</sup> Department of Chemistry, University of Delhi, Delhi 110007, India

<sup>b</sup> Department of Chemistry, R.S.S. (P.G.) College, Ghaziabad, NCR, Delhi, India

Received 21 September 2006; accepted 1 November 2006

## Abstract

A new series of complexes of 2-hydroxy-3,5-dimethyl acetophenone oxime (HDMAOX) with Cu(II), Co(II), Ni(II) and Pd(II) have been prepared and characterized by different physical techniques. Infrared spectra of the complexes indicate deprotonation and coordination of the phenolic OH. It also confirms that nitrogen atom of the oximino group contributes to the complexation. Electronic spectra and magnetic susceptibility measurements reveal square planar geometry for Cu(II), Ni(II) and Pd(II) complexes and tetrahedral geometry for Co(II) complex. The elemental analyses and mass spectral data have justified the ML<sub>2</sub> composition of complexes. Kinetic and thermodynamic parameters were computed from the thermal decomposition data using Coats and Redfern method. The geometry of the metal complexes has been optimized with the help of molecular modeling. The free ligand (HDMAOX) and its metal complexes have been tested *in vitro* against *Alternaria alternata*, *Aspergillus flavus*, *Aspergillus nidulans* and *Aspergillus niger* fungi and *Streptococcus*, *Staph*, *Staphylococcus* and *Escherchia coli* bacteria in order to assess their antimicrobial potential. The results indicate that the ligand and its metal complexes possess antimicrobial properties.

© 2006 Elsevier B.V. All rights reserved.

**Keywords:** Bioactivity; Kinetics; Metal complexes; Molecular modeling; Spectra

## 1. Introduction

Presently, there is a growing interest in the coordination chemistry of structurally modified bio-ligands. Transition metal complexes with potential biological activity are the focus of extensive investigations. Acetophenoneoxime is an important bioactive ligand for a wide variety of applications. Different oximes and their metal complexes have shown notable bioactivity as chelating therapeutics, as drugs, as inhibitors of enzymes and as intermediates in the biosynthesis of nitrogen oxides [1]. However, with increasing use of oximes as drugs and pesticides, the intake of these chemicals followed by enzymatic oxidation may result in the formation of a variety of reactive intermediates, which may lead to cell and tissue damage [2].

Acetophenone (AP, phenylmethylketone or hypnone) is used in consumer fragrances and as an industrial solvent. In general, acetophenones may serve as a novel group of useful therapeutics

against the mycobacteria [3]. Some acetophenone derivatives have antimicrobial activity against gram-positive bacteria and fungi [4] while others are used as herbicides [5]. Certain acetophenones carrying a hydroxyl group at C-2 have antimutagenic activity in salmonella typhimurium [6]. Many acetophenones occur as natural products in plants [7] and fungi [8]. Paeonol (2-hydroxy-4-methoxy acetophenone) an oral administration to rats is rapidly excreted in the urine as sulphated derivative [9]. *Ortho*-hydroxyacetophenoneoxime acts as an important analytical reagent for the gravimetric and colorimetric estimation of transition metals [10].

Spectral characterization and the kinetic calculations of thermal decomposition reactions serve as important tools for the interpretation of structures of molecules of biological and analytical importance. Therefore, we report herein the synthesis, spectral characterization (infrared, electronic, mass and <sup>1</sup>H NMR), magnetic susceptibility measurements and thermal studies of the complexes of HDMAOX with selected transition metal (II) ions. The geometry of the metal complexes has been optimized through molecular modeling studies, which involve energy minimization calculations. The present works

\* Corresponding author. Tel.: +91 27677525; fax: +91 27666250.  
E-mail address: [bibheshksingh@yahoo.co.in](mailto:bibheshksingh@yahoo.co.in) (B.K. Singh).

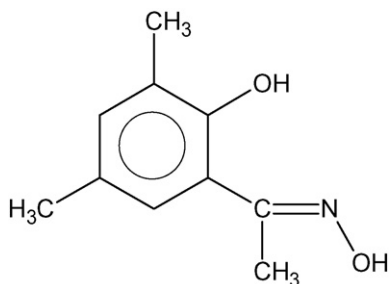


Fig. 1. Structure of 2-hydroxy-3,5-dimethylacetophenoneoxime (HDMAOX).

deals specifically the coordination properties of 2-hydroxy-3,5-dimethylacetophenoneoxime (HDMAOX) (Fig. 1) concerning its interactions with Cu(II), Co(II), Ni(II) and Pd(II). The bio-efficacy of these complexes has also been examined against the growth of bacteria and pathogenic fungi *in vitro* to evaluate their anti-microbial potential.

## 2. Experimental

### 2.1. Physicochemical studies

The stoichiometric analyses (C, H and N) of the complexes were performed using Elementar vario EL III (Germany) model. Metal contents were estimated on an AA-640-13 Shimadzu flame atomic absorption spectrophotometer in solution prepared by decomposing the respective complex in hot concentrated HNO<sub>3</sub>. Their IR spectra were recorded on Perkin-Elmer FT-IR spectrophotometer in nujol mull and polyethylene pellets. The UV–vis spectra were recorded in CDCl<sub>3</sub> on Beckman DU-64 spectrophotometer and mass spectra (TOF-MS) were recorded on Waters (USA) KC-455 model with ES<sup>+</sup> mode. <sup>1</sup>H NMR was recorded on a Bruker Advance 300 instrument. Magnetic susceptibility measurements were carried out at room temperature in powder form on a vibrating sample magnetometer PAR 155 with 5000G-field strength, using Co [Hg (SCN)<sub>4</sub>] as the calibrant (magnetic susceptibility  $\approx 1.644 \times 10^{-5} \text{ cm}^3 \text{ g}^{-1}$ ). Rigaku model 8150 thermoanalyser (Thermafex) was used for simultaneous recording of TG–DTA curves at a heating rate of  $5^\circ \text{C min}^{-1}$ . For TG, the instrument was calibrated using calcium oxalate while for DTA, calibration was done using indium metal, both of which were supplied along with the instrument in ambient condition. A flat bed type aluminium crucible was used with  $\alpha$ -alumina (99% pure) as the reference material for DTA. The number of decomposition steps was identified using TG. The activation energy (*E*) and Arrhenius constant of the degradation process was obtained by Coats and Redfern method. The initial 3D structure related to the probable geometry of each metal complex was drawn through constrain geometry and model builder option of the computer program, Hyperchem release 7.51 professional version and related minimum strain energy was calculated. The geometry of the complex was energetically optimized through molecular mechanics. Metal salts were procured from Aldrich and were used as received. Solvents used were of analytical grade and were purified by standard procedures.

### 2.2. Synthesis of the complexes

To 50 ml of 0.2 M aqueous solution of the salts of respective metal chlorides, 100 ml of 0.4 M solution of 2-hydroxy-3,5-dimethylacetophenoneoxime (HDMAOX) [11] in 50% ethanol was added. Cu(II), Co(II), Ni(II) and Pd(II) formed buff, brown, green and yellow colored precipitates in the pH range 2.5–9.0, 6.0–9.0, 5.0–9.0 and 1.5–6.5, respectively. The precipitated complexes were digested, filtered, washed first with hot water and then with 20% ethanol and finally dried at 105–110 °C in an air oven. The yields of the respective complexes were in the range of 75–85%.

### 2.3. Biological activity

#### 2.3.1. Antibacterial screening

*In vitro* anti-microbial (anti-bacterial) activities of the synthesized ligand and its metal complexes were tested using paper disc diffusion method [12]. The nutrient agar medium (peptone, beef extract, NaCl and agar-agar) and 5 mm diameter paper discs of Whatman No. 1 were used. The test compound was dissolved in methanol in 0.05–0.40% concentrations. The filter paper discs were soaked in different solutions of the compound, dried and then placed in the Petri plates (9 mm diameter) previously seeded with the test organisms *Streptococcus*, *Staph*, *Staphylococcus* and *Escherchia coli*. The plates were incubated for 24–30 h at  $27 \pm 1^\circ \text{C}$  and the inhibition zone (mm) was measured around each disc. As the organism grows, it forms a turbid layer, except in the region where the concentration of antibacterial agent is above the minimum inhibitory concentration and a zone of inhibition is seen. The size of the inhibition zone depends upon the culture medium, incubation conditions, rate of diffusion and the concentration of the antibacterial agent.

#### 2.3.2. Antifungal screening

The antifungal activity of the complexes was checked by dry weight method for the *Alternarie alternate*, *Aspergillus flavus*, *Aspergillus nidulans* and *Aspergillus niger* fungi. The complexes were directly added to the growth medium in varying concentration (0.05–0.40% (w/v)). The actively growing mycelia (of the test fungi) were placed on the medium with the help of inoculum needle and incubated at  $27 \pm 1^\circ \text{C}$  for 7 days. The medium with the test solutions served as ‘treated’ while without them as ‘control’ or ‘check’. The resulting mycelia mats in each set were carefully removed, washed, dried and then weighed separately. The fungal growth was calculated from the following relation:

$$\text{fungal growth inhibition (\%)} = \frac{C_g - T_g}{C_g} \times 100$$

where  $C_g$  is the average growth in the ‘control’ or ‘check’ set and  $T_g$  is the average growth in the treated set.

## 3. Results and discussion

On the basis of elemental analysis data (Table 1), all the complexes have the general composition  $ML_2$ , where

Table 1  
Analytical data, magnetic moment (BM) and electronic spectral data ( $\text{cm}^{-1}$ ) of the metal complexes

Sl. no.	Complex [empirical formula]	Decomposition temperature ( $^{\circ}\text{C}$ )	Yield (%)	Analysis found (calculated) (%)				$\mu_{\text{eff}}$ (BM)	Electronic spectral data ( $\text{cm}^{-1}$ )
				C	H	N	M		
(1)	Cu (HDMAOX) <sub>2</sub> [C <sub>20</sub> H <sub>24</sub> N <sub>2</sub> O <sub>4</sub> Cu]	278	83	57.18 (57.21)	5.67 (5.72)	6.60 (6.67)	15.04 (15.14)	15152, 19608, 28409, 39683	
(2)	Co (HDMAOX) <sub>2</sub> [C <sub>20</sub> H <sub>24</sub> N <sub>2</sub> O <sub>4</sub> Co]	230	80	57.80 (57.87)	5.72 (5.79)	6.71 (6.75)	14.16 (14.20)	4500, 14970, 14185, 28571, 40323	
(3)	Ni (HDMAOX) <sub>2</sub> [C <sub>20</sub> H <sub>24</sub> N <sub>2</sub> O <sub>4</sub> Ni]	300	79	57.76 (57.84)	5.71 (5.79)	6.67 (6.74)	14.07 (14.15)	15385, 16529, 18116, 27778, 32680, 40160	
(4)	Pd (HDMAOX) <sub>2</sub> [C <sub>20</sub> H <sub>24</sub> N <sub>2</sub> O <sub>4</sub> Pd]	286	78	51.83 (51.90)	5.12 (5.19)	6.01 (6.05)	22.96 (23.01)	13986, 20080, 24213, 27027, 35971, 40816	

M=Cu(II), Co(II), Ni(II) and Pd(II); L=2-hydroxy-3,5-dimethylacetophenoneoxime (HDMAOX). The complexes were obtained in powder form. These were found to be sufficiently soluble in chloroform and DMSO for spectral measurements. Various attempts to obtain the single crystals of the complexes have so far been unsuccessful.

### 3.1. IR spectra and mode of bonding

In the absence of a powerful technique such as X-ray crystallography, IR spectra have proven to be the most suitable technique to give enough information's to elucidate the nature of bonding of the ligand to the metal ion. The IR spectra of the free ligand and metal complexes (Fig. 2a–d) were carried out in the range 4000–400  $\text{cm}^{-1}$  and 400–100  $\text{cm}^{-1}$  (Table 2). The IR spectrum of the ligand shows a broad band between 3200 and 3450  $\text{cm}^{-1}$ , which can be attributed to phenolic OH group. This band disappears in all complexes, which can be attributed to the involvement of phenolic OH in coordination. The involvement of deprotonated phenolic moiety in complexes is confirmed by the shift of  $\nu(\text{C}-\text{O})$  stretching band observed at 1212  $\text{cm}^{-1}$  in the free ligand to a lower frequency to the extent of 10–20  $\text{cm}^{-1}$  [13]. The shift of  $\nu(\text{C}-\text{O})$  band at 1212  $\text{cm}^{-1}$  to a lower frequency suggests the weakening of  $\nu(\text{C}-\text{O})$  and formation of stronger M–O bond. The broad and low intensity bands due to  $\nu(\text{O}-\text{H})$  modes of N–OH groups in the 4000–3000  $\text{cm}^{-1}$  frequency range shifted to the lower frequency region (3136–3188  $\text{cm}^{-1}$ ) which suggests the weakening of N–OH bond and formation of M–N bond [1]. The medium bands observed in the 1646–1620  $\text{cm}^{-1}$  frequency ranges in complexes were assigned to  $\nu(\text{C}=\text{N})$  mode. The shift of  $\nu(\text{C}=\text{N})$  vibration in all the complexes to a lower frequency suggests that the nitrogen atom of the ring contributes to the complexation. The lower  $\nu(\text{C}=\text{N})$  frequency also indicates stronger M–N bonding [14,15].

The IR spectrum of the ligand showed that the  $\nu(\text{N}-\text{O})$  band appears at 860  $\text{cm}^{-1}$ . So, on M–N interaction,  $\nu(\text{N}-\text{O})$  appeared at higher frequencies, indicating that N–O bond length decreases. The positive  $\nu(\text{N}-\text{O})$  shift indicates strengthening of the M–N bond. In the IR spectra of the complexes, a band is observed between 430 and 460  $\text{cm}^{-1}$  that is attributed to the  $\nu(\text{M}-\text{N})$  stretching vibrations. Another band appeared between 660 and 672  $\text{cm}^{-1}$ , which is assigned to the interaction of phenolic oxygen to the metal atom, i.e., the stretching vibrations  $\nu(\text{M}-\text{O})$  [13]. The band at 1374–1376  $\text{cm}^{-1}$  in all the complexes is due to the  $\nu(\text{CH}_3)$  frequency, is not affected upon complexation. Furthermore, the aliphatic protons are not greatly affected upon complexation [16].

### 3.2. Magnetic moments and electronic spectra

Magnetic susceptibility measurements were carried out in the solid state at room temperature (25  $^{\circ}\text{C}$ ) and the results are presented in Table 1. The magnetic moments of the copper(II) and cobalt(II) complexes are 1.74 and 4.32 BM, respectively, which suggests square planar geometry for copper(II) complex and tetrahedral geometry for cobalt(II) complex. For tetrahedral

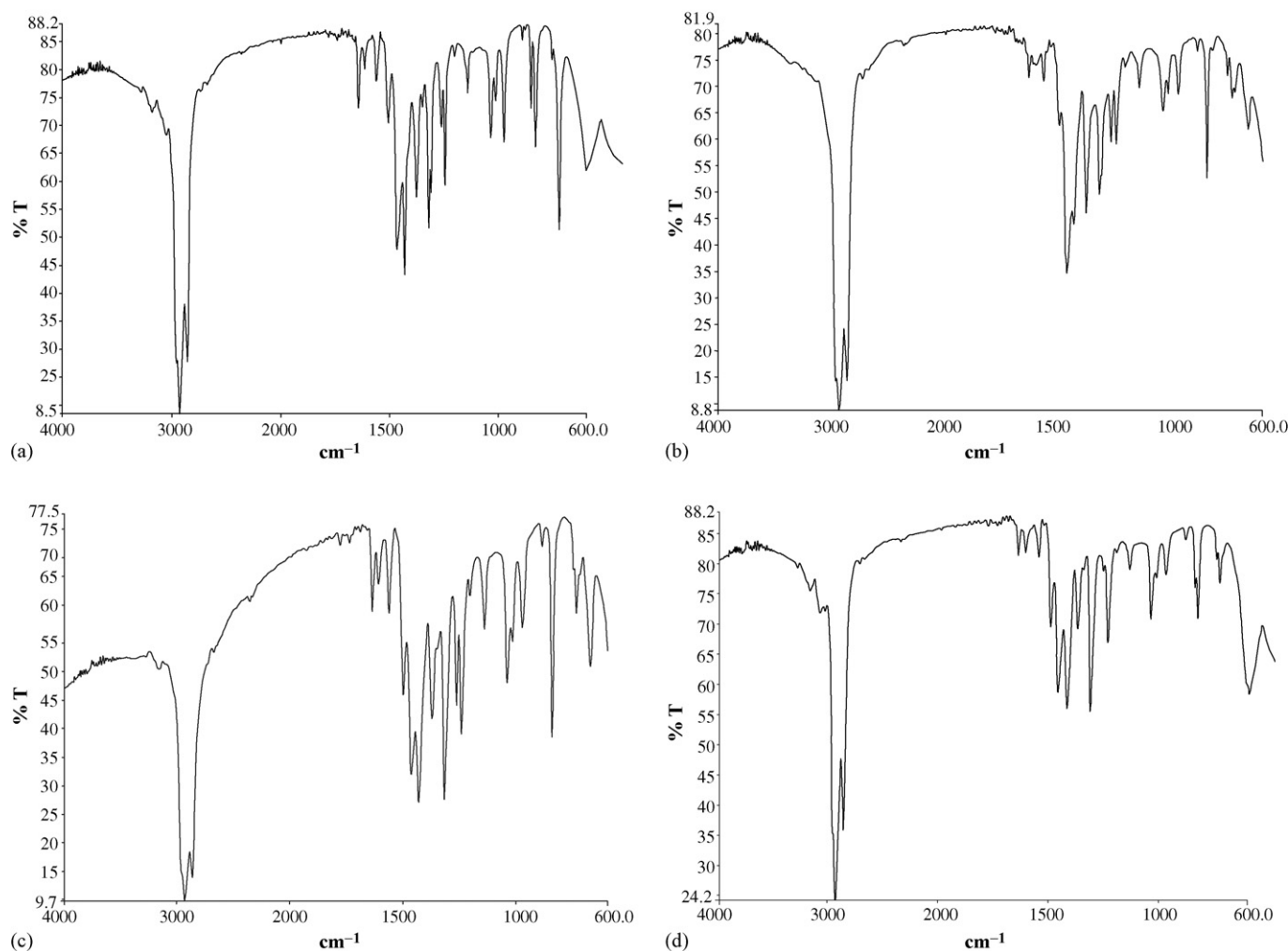


Fig. 2. (a) IR spectrum of Cu–HDMAOX complex, (b) IR spectrum of Co–HDMAOX complex, (c) IR spectrum of Ni–HDMAOX complex, and (d) IR spectrum of Pd–HDMAOX complex.

cobalt(II) complex, the state acquires orbital angular momentum only indirectly through the mixing of the  $^4T_2$  state by a spin–orbit coupling perturbation. The nickel(II) and palladium(II) complexes are diamagnetic at room temperature revealing the square planar geometry around the metal (II) ion [17]. The electronic spectra of the complexes are presented in Table 1. Two very strong bands in the region 242–252 and 345–370 nm in the

spectra of the complexes, are attributed to  $n \rightarrow \pi^*$  and  $\pi \rightarrow \pi^*$  transitions in aromatic ring and C=N chromophore [18]. The visible spectrum of copper complex (Fig. 3a), shows two absorption bands at 660 nm and 510 nm assignable to  $^2B_{1g} \rightarrow ^2B_{2g}$  and  $^2B_{1g} \rightarrow ^2E_g$  transitions respectively, which indicates the possibility of square planar geometry of the metal complex [19]. Cobalt (II) complex (Fig. 3b) shows absorption bands at

Table 2  
IR spectral data ( $\text{cm}^{-1}$ ) of metal complexes

Frequency	[Cu (HDMAOX) <sub>2</sub> ]	[Co (HDMAOX) <sub>2</sub> ]	[Ni (HDMAOX) <sub>2</sub> ]	[Pd (HDMAOX) <sub>2</sub> ]
$\nu(\text{OH})_{\text{NOH}}$	3175 (w)	3188 (w)	3142 (w)	3136 (w)
$\nu(\text{C}=\text{N})$	1641 (s)	1630 (s)	1639 (s)	1646 (s)
$\delta(\text{NOH})$	1467 (s)	1463 (s)	1463 (s)	1464 (s)
$\nu(\text{CH})$	2924 (s), 2854 (m)	2924 (s), 2855 (m)	2923 (s), 2855 (m)	2924 (s), 2855 (m)
$\nu(\text{NO})$	975	971	977	978
$\delta(\text{O}-\text{M}-\text{O})$	186	193	191	194
$\delta(\text{O}-\text{M}-\text{N})$	214	233	236	237
$\nu(\text{M}-\text{O})$	340 (m)	317 (m)	329 (m)	334(m)
$\nu(\text{M}-\text{N})$	272 (m)	285 (m)	293 (m)	287 (m)
$\nu(\text{CH}_3)$	1376	1377	1375	1376
$\nu(\text{C}-\text{O})$	1201	1204	1203	1202

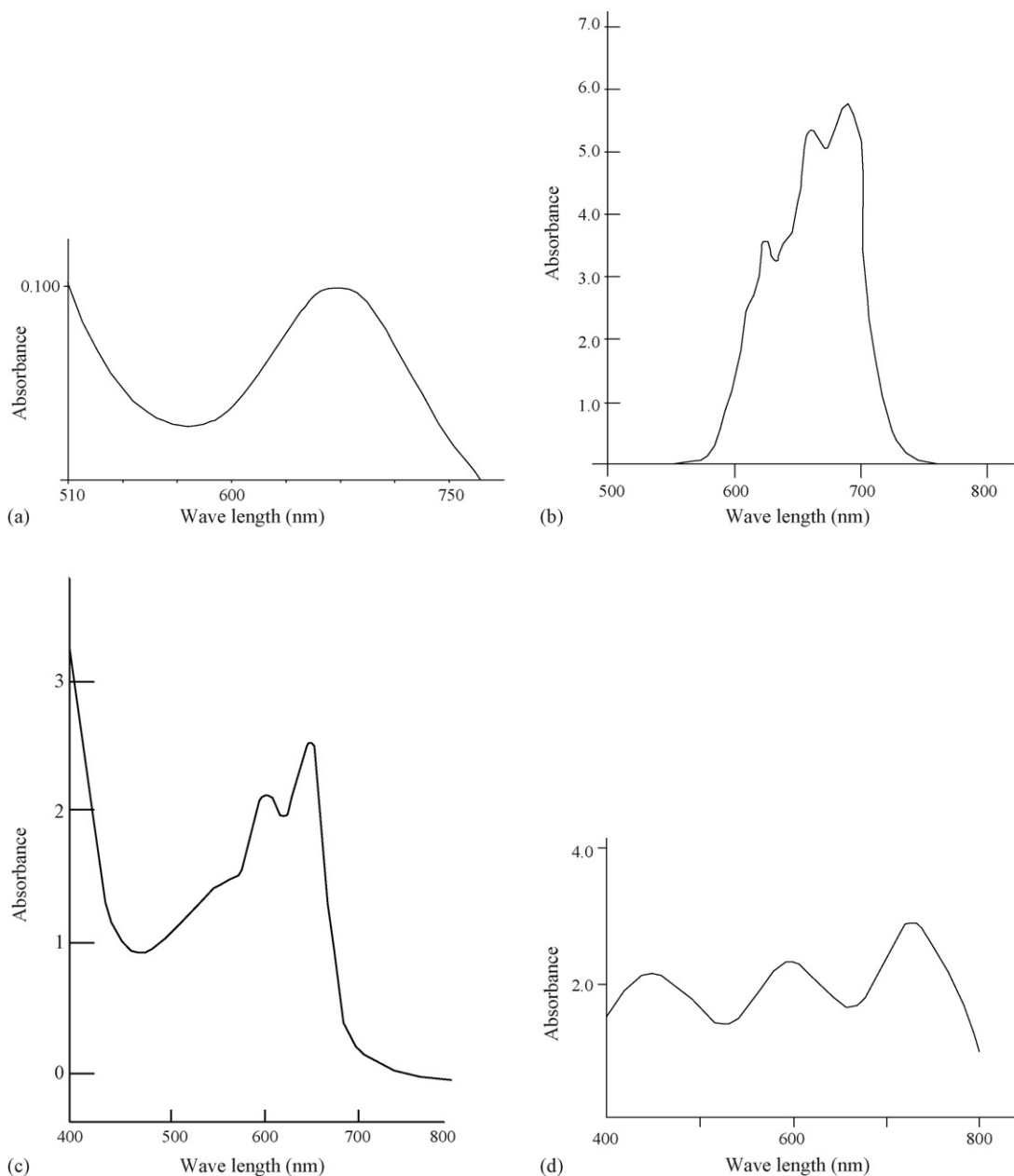


Fig. 3. (a) Electronic spectra of Cu–HDMAOX complex, (b) electronic spectra of Co–HDMAOX complex, (c) electronic spectra of Ni–HDMAOX complex, and (d) electronic spectra of Pd–HDMAOX complex.

668 nm assigned to  ${}^4A_2 \rightarrow {}^4T_1$  (P) transition. The existence of spin - orbit coupling also allows some quartet  $\rightarrow$  doublet spin transition to occur. Another band at 705 nm is assigned to  ${}^4A_2 \rightarrow {}^4T_1$  (F). The expected  ${}^4A_2 \rightarrow {}^4T_1$  transition appearing at a  $4500\text{ cm}^{-1}$  is overlapped by ligand vibration transitions (i.e., the infrared bands) suggests tetrahedral geometry of the complex [20,21], which is also corroborated by magnetic moment value of the complex. Spectra of the nickel complex (Fig. 3c) shows an absorption band at 650 nm, assignable to a  ${}^1A_{1g} \rightarrow {}^1A_{2g}$  transition and a shoulder at 552 nm corresponding to a  ${}^1A_{1g} \rightarrow {}^1B_{1g}$  transition which are consistent with square planar stereochemistry about the nickel(II) ion. Palladium complex (Fig. 3d) has three spin allowed singlet–singlet d–d transitions, which are  ${}^1A_{1g} \rightarrow {}^1A_{2g}$  (715 nm),  ${}^1A_{1g} \rightarrow {}^1B_{1g}$  (498 nm) and  ${}^1A_{1g} \rightarrow {}^1E_g$

(413 nm) [20,22]. These transitions are from the lower lying d orbital to the empty  $d_{x^2-y^2}$  orbital. The strong band at 373 nm is assignable to a combination of M  $\rightarrow$  L (charge transfer) and d–d bands.

### 3.3. Mass spectra

The recorded mass spectra of the complexes (Fig. 4a–d) and the molecular ion peaks have been used to confirm the proposed formula. Calculated and found molecular weights corresponding to the important mass peaks for the studied compounds are given in Table 3. The multi-peaks pattern of the mass spectrum gives an impression of the successive degradation of the target compound with the series of peaks corresponding to the

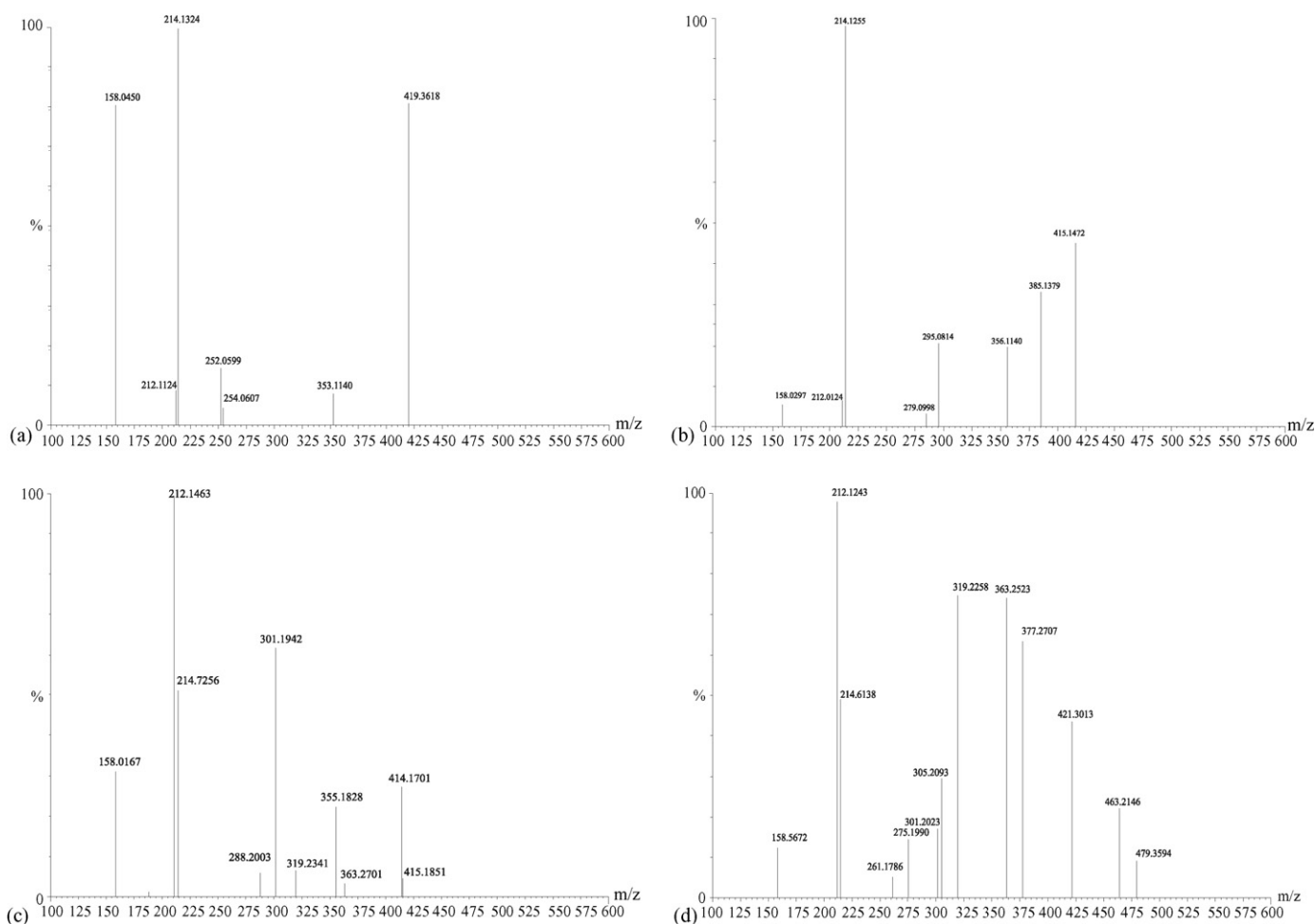


Fig. 4. (a) Mass spectra of Cu–HDMAOX complex, (b) mass spectra of Co–HDMAOX complex, (c) mass spectra of Ni–HDMAOX complex, and (d) mass spectra of Pd–HDMAOX complex.

various fragments. Their intensity gives an idea of stability of fragments. The last two fragments in all the complexes appear at positions ( $m/z$  value) 212 (100%) and 158 (<100%). These values correspond to the  $[C_{16}H_{20}]^+$  and  $[C_{12}H_{14}]^+$  fragments, respectively.

### 3.4. $^1H$ nuclear magnetic resonance spectra

The  $^1H$  NMR spectra of a DMSO- $d_6$  solution of the oxime ligand (HDMAOX) and Ni(II), Pd(II) complexes show well-resolved signals as expected. The solvent impurity resonates near 3.0. The spectrum of the oxime shows a singlet at 1.2 ppm (3H), singlet at 2.2 ppm (6H), singlet at 7.60–7.90 ppm (2H), singlet at 11.4 ppm (1H), singlet at 12.6 ppm (1H). The  $^1H$  NMR spectra of both the complexes (Fig. 5a and b) show the resonance with expected integrated intensities. In both complexes, no signal is recorded for phenolic hydrogen in the 12–13.5 ppm region, as in the case of ligand (HDMAOX). This indicates deprotonation of the *ortho*-hydroxyl group on complexation. The other resonances were observed at 0.8–1.3 ppm (6H), 2.0–2.7 ppm (12H), 6.7–8.1 ppm (4H) and 11.53 ppm (2H) corresponding to  $CH_3$ -a,  $CH_3$ -b, aromatic protons and oxime –OH proton resonances.

### 3.5. Kinetics of thermal decomposition

Recently, there has been increasing interest in determining the rate-dependent parameters of solid-state non-isothermal decomposition reactions by analysis of TG curves [23,24]. Thermogravimetric (TG) and differential thermogravimetric (DTG) analyses were carried out for Cu(II), Co(II), Ni(II) and Pd(II)–HDMAOX complexes in ambient conditions. The correlations between the different decomposition steps of the complexes with the corresponding weight losses are discussed in terms of the proposed formula of the complexes.

The complex  $[Cu(HDMAOX)_2]$  with the molecular formula  $[C_{20}H_{24}N_2O_4Cu]$  is thermally decomposed in two successive decomposition steps (Fig. 6a). The first estimated mass loss of 38.60% (calculated mass loss = 38.62%) within the temperature range 540–590 K may be attributed to the loss of  $(C_{10}H_{12}NO)$  fragment. The DTG curve gives an exothermic peak at 553 K (the maximum peak temperature). The second step occurs within the temperature range 661–853 K with the estimated mass loss 42.40% (calculated mass loss = 42.43%) which corresponds to the loss of  $C_{10}H_{12}NO_2$  fragment leaving CuO as residue. The DTG curve gives an exothermic peak at 770 K (the maximum

Table 3  
Important mass peaks for the compounds studied

	Mass assignments	<i>M</i>	<i>m/z</i>
(1)	[C <sub>20</sub> H <sub>24</sub> N <sub>2</sub> O <sub>4</sub> Cu] <sup>+</sup>	419.5	419.36
	[C <sub>17</sub> H <sub>23</sub> NO <sub>3</sub> Cu] <sup>+</sup>	352.5	353.11
	[C <sub>17</sub> H <sub>21</sub> NO] <sup>+</sup>	255.0	252.06
	[C <sub>16</sub> H <sub>20</sub> ] <sup>+</sup>	212.0	214.13
	[C <sub>12</sub> H <sub>14</sub> ] <sup>+</sup>	158.0	158.05
(2)	[C <sub>20</sub> H <sub>24</sub> N <sub>2</sub> O <sub>4</sub> Co] <sup>+</sup>	415.1	415.15
	[C <sub>20</sub> H <sub>24</sub> NO <sub>3</sub> Co] <sup>+</sup>	384.9	385.14
	[C <sub>20</sub> H <sub>24</sub> O <sub>2</sub> Co] <sup>+</sup>	354.9	356.11
	[C <sub>20</sub> H <sub>22</sub> O <sub>2</sub> ] <sup>+</sup>	294.0	295.08
	[C <sub>20</sub> H <sub>22</sub> O] <sup>+</sup>	278.0	279.09
	[C <sub>16</sub> H <sub>20</sub> ] <sup>+</sup>	212.0	214.13
	[C <sub>12</sub> H <sub>14</sub> ] <sup>+</sup>	158.0	158.02
	(3)	[C <sub>20</sub> H <sub>24</sub> N <sub>2</sub> O <sub>4</sub> Ni] <sup>+</sup>	414.9
[C <sub>20</sub> H <sub>24</sub> O <sub>2</sub> Ni] <sup>+</sup>		354.7	355.18
[C <sub>17</sub> H <sub>22</sub> ONi] <sup>+</sup>		300.9	301.19
[C <sub>16</sub> H <sub>20</sub> ] <sup>+</sup>		212.0	212.15
[C <sub>12</sub> H <sub>14</sub> ] <sup>+</sup>		158.0	158.01
(4)		[C <sub>20</sub> H <sub>24</sub> N <sub>2</sub> O <sub>4</sub> Pd] <sup>+</sup>	462.4
	[C <sub>19</sub> H <sub>23</sub> NO <sub>3</sub> Pd] <sup>+</sup>	419.4	421.30
	[C <sub>18</sub> H <sub>22</sub> O <sub>2</sub> Pd] <sup>+</sup>	376.4	377.27
	[C <sub>17</sub> H <sub>20</sub> O <sub>2</sub> Pd] <sup>+</sup>	362.4	363.25
	[C <sub>16</sub> H <sub>20</sub> Pd] <sup>+</sup>	319.23	318.4
	[C <sub>16</sub> H <sub>20</sub> ] <sup>+</sup>	212.0	212.01
	[C <sub>12</sub> H <sub>14</sub> ] <sup>+</sup>	158.0	158.56

peak temperature). Total estimated mass loss is 81.00% (calculated mass loss = 81.05%).

The thermal decomposition of [Co (HDMAOX)<sub>2</sub>] complex (Fig. 6b) with the molecular formula [C<sub>20</sub>H<sub>24</sub>N<sub>2</sub>O<sub>4</sub>Co] proceeds with two main degradation steps. The first step occurs within the temperature range 485–590 K with an estimated mass loss 31.95% (calculated mass loss = 32.00%) which is reasonably accounted for the loss of C<sub>8</sub>H<sub>7</sub>NO fragment. The DTG curve gives an exothermic peak at 638 K (the maximum peak temperature). The second step occurs within the temperature range 595–795 K with an estimated mass loss 50.25% (calculated mass loss = 50.00%), which is reasonably accounted for the loss of rest of the ligand molecule, leaving CoO as residue. The DTG curve gives an exothermic peak at 705 K (the maximum peak temperature). Total estimated mass loss is 82.20% (calculated mass loss = 82.00%).

The thermal decomposition of [Ni (HDMAOX)<sub>2</sub>] complex (Fig. 6c) with the molecular formula [C<sub>20</sub>H<sub>24</sub>N<sub>2</sub>O<sub>4</sub>Ni] also proceeds with two main degradation steps. The first estimated mass loss of 19.90% (calculated mass loss = 20.00%) within the temperature range 592–625 K could be attributed to the liberation of C<sub>4</sub>H<sub>5</sub>NO fragment. The DTG curve gives an exothermic peak at 596 K (the maximum peak temperature). The second step occurs within the temperature range 650–815 K with an estimated mass loss 61.50% (calculated mass loss = 61.95%), which is reasonably accounted for the decomposition of remaining part of the ligand molecule (C<sub>16</sub>H<sub>19</sub>NO<sub>2</sub>) leaving NiO as residue. The DTG curve gives an exothermic peak at 760 K (the maximum peak temperature). Total estimated mass loss is 81.40% (calculated mass loss = 81.95%).

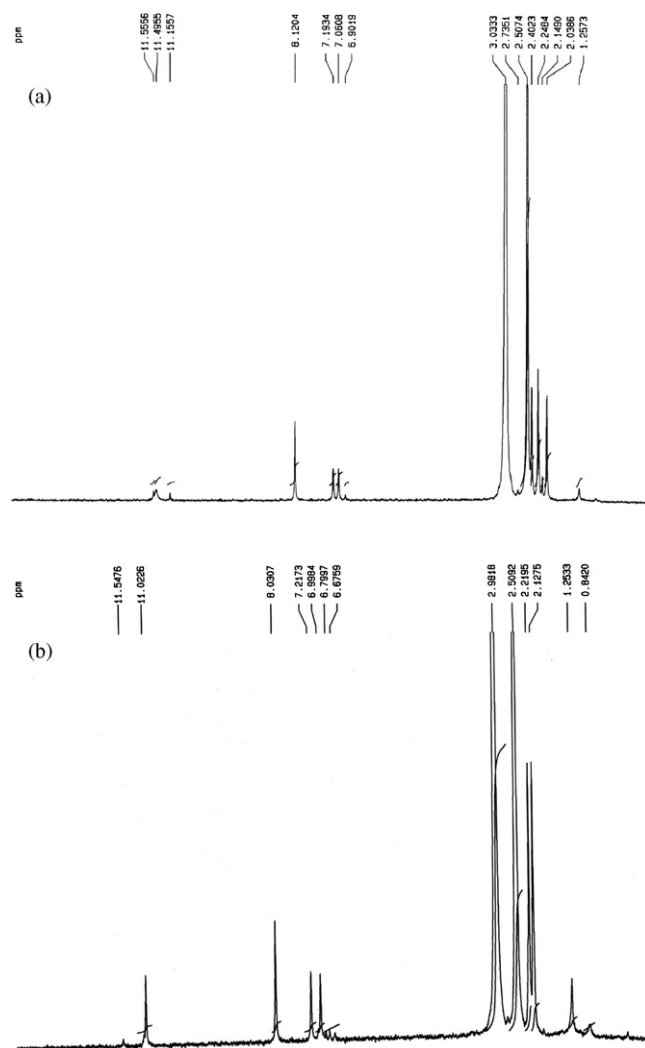


Fig. 5. (a) NMR spectra of Ni-HDMAOX complex and (b) NMR spectra of Pd-HDMAOX complex.

The [Pd (HDMAOX)<sub>2</sub>] complex (Fig. 6d) with the molecular formula [C<sub>20</sub>H<sub>24</sub>N<sub>2</sub>O<sub>4</sub>Pd] is thermally decomposed in two successive steps. The first estimated mass loss 35.00% (calculated mass loss = 35.03%) within the temperature range 558–579 K can be attributed to the loss of (C<sub>10</sub>H<sub>12</sub>NO) fragment. The DTG curve gives an exothermic peak at 568 K (the maximum peak temperature). The second step occurs within the temperature range 593–698 K with an estimated mass loss 38.48% (calculated mass loss = 38.53%), which is reasonably accounted for the loss of rest of the ligand molecule (C<sub>10</sub>H<sub>12</sub>NO<sub>2</sub>), leaving PdO as residue with total estimated mass loss of 73.48% (calculated mass loss = 73.53%). The DTG curve gives an exothermic peak at 659 K (the maximum peak temperature).

The final product of decomposition at 875 K corresponds to the formation of metal oxide as the end product, which was confirmed by comparing the observed/estimated and the calculated mass of the pyrolysis product.

The kinetic analysis parameters such as activation energy ( $\Delta E^*$ ), enthalpy of activation ( $\Delta H^*$ ), entropy of activation ( $\Delta S^*$ ), free energy change of decomposition ( $\Delta G^*$ ) were evalu-

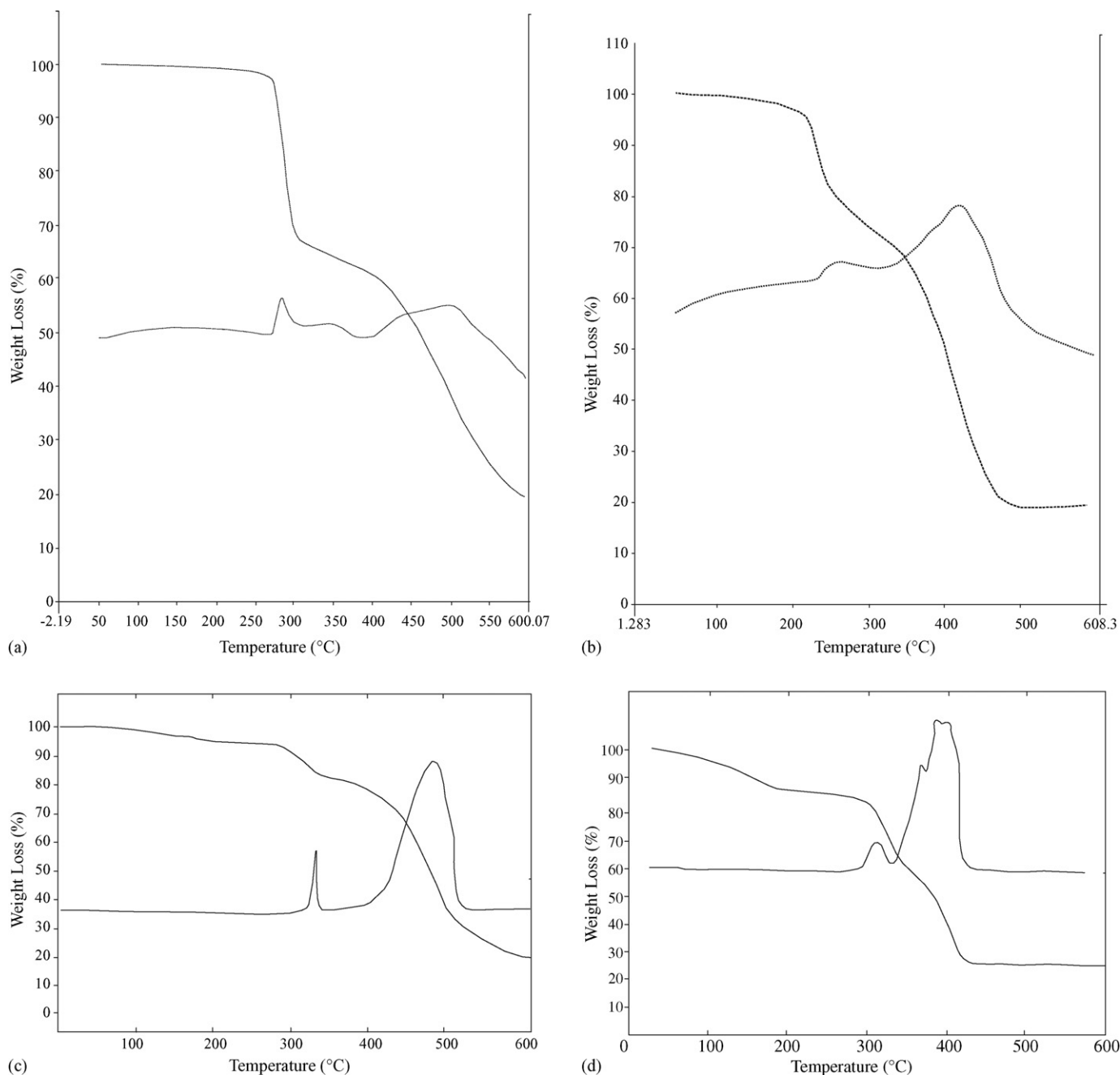


Fig. 6. (a) TG–DTG curves of the Cu–HDMAOX complex, (b) TG–DTG curves of the Co–HDMAOX complex, (c) TG–DTG curves of the Ni–HDMAOX complex, and (d) TG–DTG curves of the Pd–HDMAOX complex.

ated graphically by employing the Coats–Redfern relation [25]:

$$\log \left[ -\frac{\log(1-\alpha)}{T^2} \right] = \log \left[ \frac{AR}{\theta E^*(1-2RT/E^*)} \right] - \frac{E^*}{2.303RT} \quad (1)$$

where  $\alpha$  is the mass loss up to the temperature  $T$ ,  $R$  the gas constant,  $E^*$  the activation energy in  $\text{J mol}^{-1}$ ,  $\theta$  the linear heating rate and the term  $(1-2RT/E^*) \cong 1$ . A straight line plot of left-hand side of Eq. (1) against  $1/T$  gives the value of  $E^*$  while its intercept corresponds to  $A$  (Arrhenius constant). The linearization plots (Fig. 7(a–d)), confirms the first-order kinetics for the decomposition process. The calculation of heat of reaction ( $\Delta H^*$ ) (Table 4)

from the DTA curves was done by using the relation:

$$\Delta H^* = \Delta H(\text{muv}) 60 \times 10^{-6} (\text{MJ mol}^{-1}) \quad (2)$$

where  $M$  is the molar mass of the complex and  $\text{muv}$  = micro unit volt. The entropy of activation ( $\Delta S^*$ ) and the free energy change of activation ( $\Delta G^*$ ) were calculated using Eqs. (2) and (3):

$$\Delta S^* = 2.303R \left[ \log \left( \frac{Ah}{kT} \right) \right] (\text{JK}^{-1} \text{mol}^{-1}) \quad (3)$$

$$\Delta G^* = \Delta H^* - T\Delta S^* (\text{J mol}^{-1}) \quad (4)$$

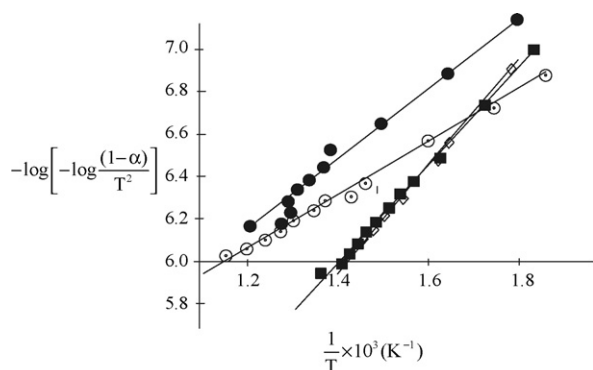


Fig. 7. Linearization plot of (a) (○) Cu-HDMAOX complex, (b) (■) Co-HDMAOX complex, (c) (●) Ni-HDMAOX complex, and (d) (◇) Pd-HDMAOX complex.

where  $k$  and  $h$  are the Boltzman and Plank constants respectively. The calculated values of  $E^*$ ,  $A$ ,  $\Delta S^*$ ,  $\Delta H^*$  and  $\Delta G^*$  for the decomposition steps of the complexes are appended in Table 4. According to the kinetic data obtained from the TG curves, all the complexes have a negative entropy which indicates that the complexes are formed spontaneously. The negative value of entropy also indicates a more ordered activated state that may be possible through the chemisorption of oxygen and other decomposition products. The negative values of the entropies of activation are compensated by the values of the enthalpies of activation, leading to almost the same values for the free energy of activation [26].

### 3.6. Molecular modeling

The molecular modeling calculations for Cu(II), Co(II), Ni(II) and Pd(II)-HDMAOX complexes were carried out using a Hyperchem program that allows for rapid structure building, geometry optimization and molecular display [27]. Molecular mechanics calculate the steric energy, which partition into stretching, bending, torsion and non-bonded interactions for the molecules and gives a stable structure with least strain energy. It provides an ideal, computationally efficient tool to evaluate the degree to which a ligand is structurally organized for metal

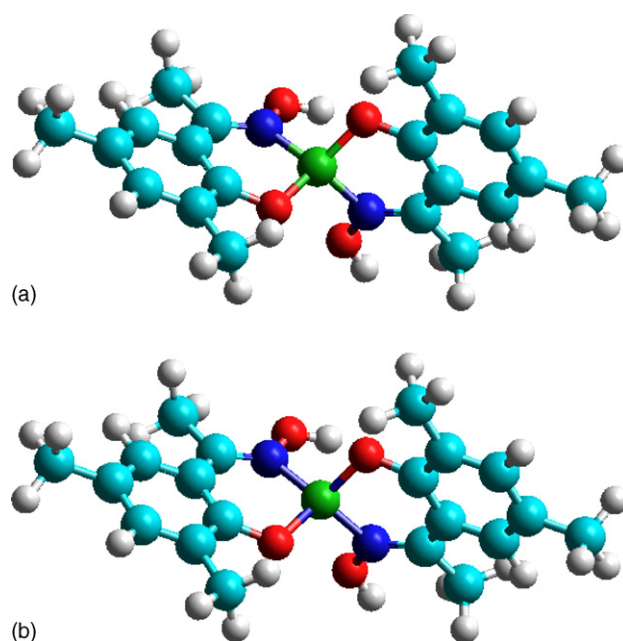


Fig. 8. (a) Optimized structure of Cu-HDMAOX complex and (b) optimized structure of Co-HDMAOX complex.

complexation. Energy minimization was repeated several times to find the global minimum. The computational strategy in this study is to determine the minimum strain energy for Cu(II), Ni(II) and Pd(II)-HDMAOX complexes, the energy minimization values for square planar and without restricting the structure are almost equal i.e., 4.91, 4.44 and 34.06 kcal/mol, respectively, whereas for Co(II)-HDMAOX complex, the energy minimization values for tetrahedral and without restricting the structure are almost equal, i.e., 4.98 kcal/mol. This supports square planar geometry for Cu(II), Ni(II) and Pd(II)-HDMAOX complexes and tetrahedral geometry for Co(II)-HDMAOX complex. Some important calculated bond length for Cu (HDMAOX)<sub>2</sub> is Cu–N, 1.831 Å; Cu–O, 1.769 Å; N–O (oxime), 1.298 Å and for Co (HDMAOX)<sub>2</sub> is Co–N, 1.832 Å; Co–O, 1.769 Å; N–O (oxime), 1.300 Å. Fig. 8(a) and (b) shows the energy-minimized structure of Cu(II) and Co(II)-HDMAOX complex.

Table 4  
Thermodynamic activation parameters of metal complexes

Complex	Order ( $n$ )	Steps	$E^*$ (J mol <sup>-1</sup> )	$A$ ( $\times 10^5$ s <sup>-1</sup> )	$\Delta S^*$ (J K <sup>-1</sup> mol <sup>-1</sup> )	$\Delta H^*$ (J mol <sup>-1</sup> )	$\Delta G^*$ (kJ mol <sup>-1</sup> )
[Cu (HDMAOX) <sub>2</sub> ]	1	I	22.97	0.27	-184.13	185.93	102.07
		II	24.88	0.25	-168.33	1245.84	130.93
[Co (HDMAOX) <sub>2</sub> ]	1	I	45.03	0.26	-165.03	95.55	88.93
		II	45.11	0.20	-169.45	1967.98	121.38
[Ni(HDMAOX) <sub>2</sub> ]	1	I	33.86	0.64	-158.57	132.27	96.57
		II	32.65	0.47	-162.98	2582.03	126.45
[Pd (HDMAOX) <sub>2</sub> ]	1	I	45.93	0.20	-168.01	272.01	99.90
		II	46.78	0.19	-169.31	2834.81	114.34

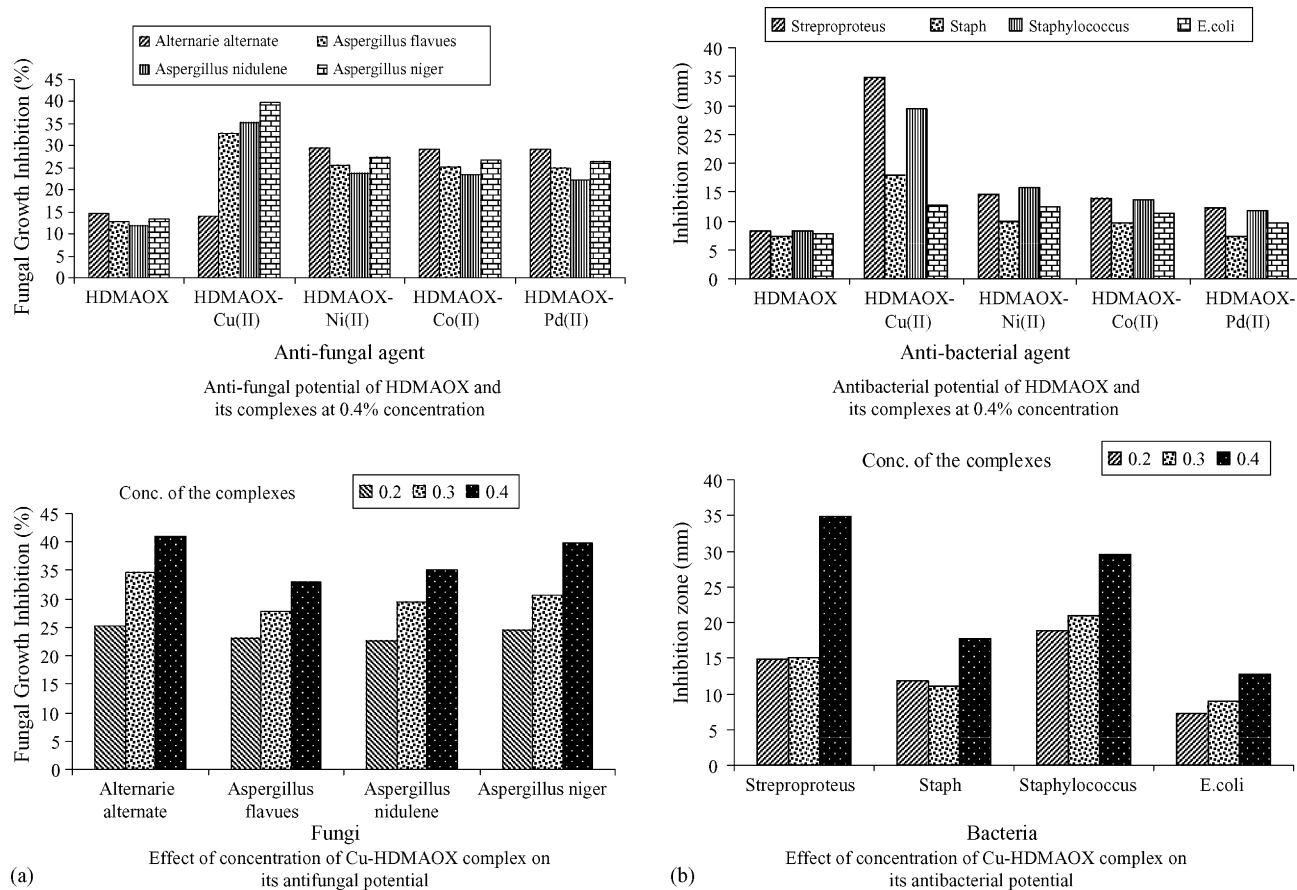


Fig. 9. (a) Anti-fungal screening and (b) anti-bacterial screening.

### 3.7. Antimicrobial activities

The free ligand and its respective metal chelates were screened against *A. alternate*, *A. flavus*, *A. nidulencia* and *A. niger* fungi and *Streptoproteus*, *Staph*, *Staphylococcus* and *E. coli* bacteria to assess their potential antimicrobial agents. The results are quite promising. It is clear from the antifungal screening data (Fig. 9a), that the metal complexes are more fungitoxic than the chelating agent itself. The bacterial screening results (Fig. 9b) reveal that the free ligand (HDMAOX) showed the maximum activity against *Streptoproteus* bacteria. Its copper, cobalt and palladium complexes also showed the maximum activity against *Streptoproteus* bacteria whereas the nickel complex showed the maximum activity against *Staphylococcus* bacteria. In general, the activity was the least against *Staph* bacteria.

The antimicrobial data reveal that the complexes are more bioactive than the free ligand. The enhanced activity of the metal complexes may be ascribed to the increased lipophilic nature of these complexes arising due to chelation [28]. It was also noted that the toxicity of the metal chelates increases on increasing the metal ion concentration. It is probably due to faster diffusion of the chelates as a whole through the cell membrane or due to the chelation theory. The bounded metal may block enzymatic activity of the cell or else it may catalyze toxic reactions among cellular constituents.

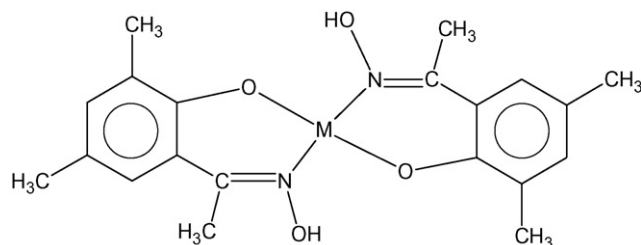


Fig. 10. Proposed structure of metal-HDMAOX complexes, where M = Cu(II), Co(II), Ni(II) and Pd(II).

It can be concluded from all the results given above that the ligand acts as bidentate chelating agent, coordinates with transition metal ions to give square planar/tetrahedral environments, around the metal ion anchor. The metal chelates of HDMAOX possess reasonable antimicrobial potential. The proposed structure of the complexes (Fig. 10).

### Acknowledgements

One of the authors (B.K. Singh) is thankful to University Grants Commission, New Delhi, India for financial assistance under research award scheme. The author UKJ is thankful to the Principal, R.S.S. (P.G.) College, Ghaziabad (NCR, Delhi), India, for providing necessary lab facilities.

## References

- [1] I. Georgieva, N. Tredafilova, G. Bauer, *Spectrochim. Acta A* 63 (2006) 403.
- [2] A. Park, N.M. Kosareff, J.S. Kim, H.J. Peter de Lijser, *Photochem. Photobiol.* 82 (2006) 110.
- [3] L. Rajabi, C. Courreges, J. Montoya, R.J. Aguilera, T.P. Primm, *Lett. Appl. Microbiol.* 40 (2005) 212.
- [4] H.I. Gul, A.A. Denizci, E. Erciyas, *Arzneimittel Forschung* 52 (2002) 773.
- [5] M. Teruyuki, H. Yoshiharu, Y. Ka, Oxime derivative thereof, Process for preparing thereof, Herbicidal composition and methods for the destruction of undesirable weeds, Asahi Chemical Ind., Japan, 1986.
- [6] M. Miyazawa, H. Shimamura, S. Nakamura, *J. Agric. Food Chem.* 48 (2000) 4377.
- [7] C. Guyot, A. Bouseta, V.V. Scheirman, *J. Agric. Food Chem.* 46 (1998) 625.
- [8] C.K. Wilkins, S. Scholl, *Int. J. Food Microbiol.* 8 (1989) 11.
- [9] T. Yasuda, R. Kon, T. Nakazawa, K. Ohsawa, *J. Nat. Product* 62 (1999) 1142.
- [10] S.N. Poddar, *Analyt. Bioanalyt. Chem.* 154 (1957) 254.
- [11] W. Nogami, *J. Pharm. Soc. Jpn.* 61 (1941) 46.
- [12] C. Saxena, D.K. Sharma, R.V. Singh, *Phosphorus Sulfur Silicon* 85 (1993) 9.
- [13] M.M. Omar, G.G. Mohamed, *Spectrochim. Acta A* 61 (2005) 929.
- [14] K. Nakamoto, *Infrared and Raman Spectra of Inorganic and Coordination Compounds*, Wiley, New York, 1978.
- [15] R.M. Silverstein, O.G. Bassler, T.C. Morrill, *Spectrophotometric Identification of Organic Compounds*, Wiley, New York, 1974.
- [16] N.M. Shauib, A.-Z.A. Elassar, A. El-Dissouky, *Spectrochim. Acta A* 63 (2006) 714.
- [17] B.N. Figgis, *Introduction to Ligand Fields*, 1st ed., 1966.
- [18] D.H. Williams, I. Fleming, *Spectrophotometric Methods in Organic Chemistry*, 4th ed., McGraw-Hill, London, 1989.
- [19] T.P. Chessman, D. Hall, T.N. Waters, *J. Chem. Soc. A* (1966) 694.
- [20] M. Ciampolini, *Struct. Bonding* 6 (1969) 52.
- [21] K. Nakamoto, S.J. McCarthy, *Spectroscopy & Structure of Metal Chelate Compounds*, John Wiley & Sons, USA, 1968.
- [22] K.I. Goldberg, J.V. Martinez, G.E. Perez, L.A. Ackerman, D.X. West, *Polyhedron* 18 (1999) 1177.
- [23] B.K. Singh, R.K. Sharma, B.S. Garg, *J. Therm. Anal. Catal.* 84 (2006) 593.
- [24] B.K. Singh, P. Mishra, B.S. Garg, *Spectrochim. Acta A* (2006) (on line available).
- [25] A.W. Coats, J.P. Redfern, *Nature* 68 (1964) 201.
- [26] B.K. Singh, R.K. Sharma, B.S. Garg, *Spectrochim. Acta A* 63 (2006) 96.
- [27] Hyperchem Release 7.51 Professional Version for Windows, Molecular Modeling System, Hyperchem Inc. Canada, 2005.
- [28] L.D.S. Yadav, S. Singh, *Ind. J. Chem. B* 40 (2001) 440.